ADVANCES IN ATMOSPHERIC SCIENCES, VOL. 39, NOVEMBER 2022, 1969–1981

• **Original Paper** •

Sub-seasonal Prediction of the South China Sea Summer Monsoon Onset in the NCEP Climate Forecast System Version 2

Weiwei WANG[1], Song YANG[*1,2], Tuantuan ZHANG[1,2], Qingquan LI[3], and Wei WEI[1,2]

[1]*School of Atmospheric Sciences and Guangdong Province Key Laboratory for Climate Change and Natural Disaster Studies, Sun Yat-sen University, Zhuhai* 519082, *China*

[2]*Southern Marine Science and Engineering Guangdong Laboratory (Zhuhai), Zhuhai* 519082, *China*

[3]*National Climate Center, China Meteorological Administration, Beijing* 100081, *China*

(Received 28 October 2021; revised 18 March 2022; accepted 29 March 2022)

ABSTRACT

This study depicts the sub-seasonal prediction of the South China Sea summer monsoon onset (SCSSMO) and investigates the associated oceanic and atmospheric processes, utilizing the hindcasts of the National Centers for Environmental Prediction (NCEP) Climate Forecast System version 2 (CFSv2). Typically, the SCSSMO is accompanied by an eastward retreat of the western North Pacific subtropical high (WNPSH), development of the cross-equatorial flow, and an increase in the east-west sea surface temperature (SST) gradient. These features are favorable for the onset of westerlies and strengthening of convection and precipitation over the South China Sea (SCS). A more vigorous SCSSMO process shows a higher predictability, and vice versa. The NCEP CFSv2 can successfully predict the onset date and evolution of the monsoon about 4 pentads (20 days) in advance (within 1–2 pentads) for more forceful (less vigorous) SCSSMO processes. On the other hand, the climatological SCSSMO that occurs around the 27th pentad can be accurately predicted in one pentad, and the predicted SCSSMO occurs 1–2 pentads earlier than the observed with a weaker intensity at longer leadtimes. Warm SST biases appear over the western equatorial Pacific preceding the SCSSMO. These biases induce a weaker-than-observed WNPSH as a Gill-type response, leading to weakened low-level easterlies over the SCS and hence an earlier and less vigorous SCSSMO. In addition, after the SCSSMO, remarkable warm biases over the eastern Indian Ocean and the SCS and cold biases over the WNP induce weaker-than-observed westerlies over the SCS, thus also contributing to the less vigorous SCSSMO.

Key words: South China Sea summer monsoon onset, sub-seasonal prediction, the NCEP CFSv2

Citation: Wang, W. W., S. Yang, T. T. Zhang, Q. Q. Li, and W. Wei, 2022: Sub-seasonal prediction of the South China Sea summer monsoon onset in the NCEP Climate Forecast System Version 2. *Adv. Atmos. Sci.*, **39**(11), 1969−1981, https://doi.org/10.1007/s00376-022-1403-0.

Article Highlights:

- The NCEP CFSv2 can accurately predict the climatological SCSSMO one pentad in advance.
- SST biases in the Indian Ocean and the western Pacific jointly affect the prediction skills of SCSSMO by the CFSv2.
- A vigorous SCSSMO process shows higher predictability and vice versa.

1. Introduction

The South China Sea (SCS) summer monsoon onset (SCSSMO) has been regarded as the first onset of the East Asian summer monsoon system (Tao and Chen, 1987; Lau and Yang, 1997; Lau et al. 1998; Ding et al., 2004; Ding and Chan, 2005). The SCSSMO is characterized by an abrupt reversal of the low-level zonal winds from easterlies to westerlies and an outbreak of the rainy season over the SCS (Wang et al., 2004). Monsoon precipitation acts as a heat source, which further exerts influences on the weather and climate over East Asia, India, and Australia (e.g., Wang et al., 2008, 2009, 2021). The pan-SCS area provides major sources of raw materials, agricultural products, and industrial outputs, and improvement of the SCSSMO prediction is crucial for agriculture and socioeconomic planning for East and Southeast Asian countries (Lau and Yang, 1997).

Typically, the SCSSMO is accompanied by an eastward withdrawal of the northwestern Pacific subtropical high (WNPSH) in the mid-lower troposphere (e.g., Ding and Sun, 2001; Wang et al., 2009; Liu and Zhu, 2019). The intrasea-

* Corresponding author: Song YANG
Email: yangsong3@mail.sysu.edu.cn

sonal variability of atmospheric circulation and convection can trigger the SCSSMO in the winter-to-summer transition episode, by modulating the WNPSH (Wu and Zhang, 1998; Jia et al., 2021; Liu and Zhu, 2021). In addition, the SCSSMO can also be modulated by local sea surface temperature (SST) in the SCS (Chen and Wang, 1998; Ding et al., 2004; He and Wu, 2013) and the western Pacific warm pool (Chen and Hu, 2003; Kajikawa and Wang, 2012; Zhao et al., 2015; Lin and Zhang, 2020). The deep convection over the Bay of Bengal and the land-sea thermal contrast between the Indo-China Peninsula and the SCS also play important roles in the SCSSMO (Wu et al., 2005; Li et al., 2020).

While much progress has been made in understanding the mechanism for the SCSSMO, challenges remain in successfully predicting the onset date of the regional monsoon. The evolution process of the SCSSMO varies among cases. For example, the SCSSMO in 2018 following a La Niña event was extremely late (Liu and Zhu, 2019). In 2019, the SCSSMO was advanced by a tropical cyclone over the Bay of Bengal and its upscaling effect on the diabatic heating of the Tibetan Plateau, which resulted in enhancement and northward shift of the South Asian High (Hu et al., 2020b; Liu and Zhu, 2020, 2021). By establishing different statistical models, Zhu and Li (2017) and Geen (2021) showed competitive skills for predicting the SCSSM onset, but these prediction skills varied year by year.

Numerical models provide another option for monsoon prediction. For example, the National Centers for Environmental Prediction (NCEP) Climate Forecast System (CFS), which is one of the state-of-the-art operational climate forecast systems, showed reasonable skills in predicting the East and Southeast Asian summer monsoon (e.g., Yang et al., 2008; Liang et al., 2009; Jiang et al., 2013; Liu et al., 2013; Zuo et al., 2013). Yang et al. (2008) indicated that the NCEP CFS successfully simulated the major features of the Asian summer monsoon, including the climatological location and interannual variability of major precipitation centers and associated atmospheric circulation systems. The air-sea interaction processes associated with the Asian summer monsoon precipitation are also well captured by the CFS (Liang et al., 2009; Dong et al., 2020). In addition, the CFS version 2 (CFSv2) can successfully predict sub-seasonal-to-seasonal features of the early season rainfall and associated circulation patterns over southern China when the forecast lead time is less than two weeks (Zhao and Yang, 2014; Zhao et al., 2015; Li et al., 2022). The predictability of the subtropical Asian summer rain band and the Maritime Continent rainfall in the NCEP CFS has also been evaluated (Gao et al., 2011; Zhang et al., 2016; Wang et al., 2017).

Although previous studies have demonstrated that the year-to-year variation of the SCSSMO can be skillfully predicted by dynamic models (i.e., GloSea5 seasonal forecasting system) up to three months in advance (Martin et al., 2019), and the operational European Centre for Medium-range Weather Forecasts sub-seasonal-to-seasonal forecasting system provides accurate prediction of the SCSSMO date 10 days in advance (Yan et al., 2021), the sub-seasonal prediction of the SCSSMO still requires further study. In this study, we investigate the sub-seasonal prediction of the SCSSMO and its responsible physical mechanisms using the NCEP CFSv2. We intend to address the following questions: To what extent can the CFSv2 predict the SCSSMO? What are the underlying mechanisms responsible for the sub-seasonal prediction of the SCSSMO? What are the factors that affect the predictability of the SCSSMO?

The rest of this paper is organized as follows. The model, data and analysis methods applied in this study are described in section 2. In section 3, we assess the major features of the SCSSMO and associated atmospheric circulation in observations and in the CFSv2 at the 0-day lead. We discuss the capabilities of the CFSv2 in predicting the climatic SCSSMO and associated atmospheric and oceanic processes at various lead times in section 4. The year-to-year variability of the sub-seasonal prediction skill of the CFSv2 for SCSSMO cases is presented, and the predictability of the SCSSMO is also discussed in section 5. Finally, a summary of the study and further discussions are provided in section 6.

2. Data and methods

The NCEP CFSv2 is a state-of-the-art, fully-coupled land-ocean-atmosphere dynamic prediction system, providing an operational prediction of the world's climate (Saha et al., 2014). Its atmospheric component is the NCEP Global Forecast System, with a T126 resolution in the horizontal and 64 sigma layers in the vertical (Moorthi et al., 2001). Its land component is the NCEP/Oregon State University/Air Force/Hydrologic Research Laboratory land model (Ek et al., 2003) and the ocean component is the Modular Ocean Model version 4.0 from the NOAA Geophysical Fluid Dynamics Laboratory (Griffies et al., 2003). The daily outputs of upward long-wave radiation (OLR), 850-hPa and 200-hPa winds, rainfall, 500-hPa geopotential height, and sea surface temperature (SST) from the retrospective forecasts with 45-day integrations of the CFSv2 from 1999 to 2014 were analyzed in this study. The hindcast runs were initialized at 0000, 0600, 1200, and 1800 UTC, and the lead time for a target day was as large as 44 days. The 0-day (44-day) lead denotes that the model runs were initialized on the current day (44 days ago). More details about the CFSv2 can be found at http://cfs.ncep.noaa.gov/cfsv2.info/. For convenience, LD0, LD1, LD2, …, and LD44 represent the outputs of 0-day lead, 1-day lead, 2-day lead, …, and 44-day lead, respectively. For a specific lead time of the pentad mean, all the five days are calculated from the same lead.

The observational data used for model verification comprise daily OLR, 850-hPa and 200-hPa winds, rainfall, and 500-hPa geopotential height from the NCEP–NCAR (National Center for Atmospheric Research) reanalysis (Kalnay et al., 1996) with a horizontal resolution of 2.5°, and the daily SST with a horizontal resolution of 0.25° from

the NOAA optimally interpolated SST analysis version 2 (OISSTv2) (Reynolds et al., 2007). Daily mean and 5-day (pentad) mean data were utilized. The detrended Niño-3.4 index data were extracted from NOAA's Climate Prediction Center data.

The SCSSM index was constructed by the area-averaged 850-hPa zonal winds over 5°–15°N, 110°–120°E (U_{SCS}), following Wang et al. (2004). The date of SCSSMO is defined as the first pentad after 25 April that satisfies the following two criteria: 1) At the onset pentad, $U_{SCS} > 0$; and 2) in the subsequent four pentads (including the onset pentad), U_{SCS} must be positive in at least three pentads and the accumulative four-pentad mean $U_{SCS} > 1$ m s^{-1} (Wang et al., 2004).

3. Atmospheric and oceanic processes associated with SCSSMO and its simulation in LD0

Figure 1 shows the time-latitude cross section of climatological rainfall and atmospheric circulation along 110°–120°E from the 12th pentad to the 42nd pentad. In the lower troposphere, the easterlies over the SCS switch to westerlies around the 27th pentad (Fig. 1a). Meanwhile, the OLR below 235 W m^{-2} expands northward to 15°N, accompanied by rainfall enhancement (above 6 mm d^{-1}) between 5° and 15°N (Figs. 1a and b). Apparently, these features signify a SCSSMO. Correspondingly, the WNPSH (marked by the 5880 gpm geopotential height) vanishes from the SCS (Fig. 1a). In the upper troposphere, westerlies weaken from the 12th pentad to the 32nd pentad and then reverse to easterly wind north of 20°N (Fig. 1b).

Figure 2a shows the climatological (1999–2014) daily SCSSM index from the 24th pentad to the 30th pentad, in which the black line denotes observed values. In climatology the daily SCSSM index is negative before the 26th pentad, converting to a positive value during the 26th–27th pentads (Fig. 2a). The positive value of the SCSSM index is maintained for at least 5 pentads. According to the definition, the climatological date of SCSSMO is the 27th pentad.

Sub-seasonal evolutions of OLR, precipitation, 500-hPa geopotential height, 850-hPa and 200-hPa winds, and SST are shown in Fig. 3. On the 25th pentad (before the SCSSMO), the SCS and the northwestern Pacific are controlled by the WNPSH, which induces low-level easterlies over the SCS (Fig. 3a). Southwesterlies induced by the cross-equatorial flow prevail from the equatorial western IO to the Indo-China Peninsula (Fig. 3a). Corresponding to the large-scale circulation, convection and heavy rainfall appear over the central and eastern IO, and the Maritime Continent. The SST above 30°C is observed over the Bay of Bengal, warmer than the SSTs on its two flanks (Fig. 3i). This zonal SST gradient leads to easterlies (westerlies) to the east (west) of Bay of Bengal, as observed in Fig. 3a. On the 27th pentad (the SCSSMO), the WNPSH retreats to the east of 120°E,

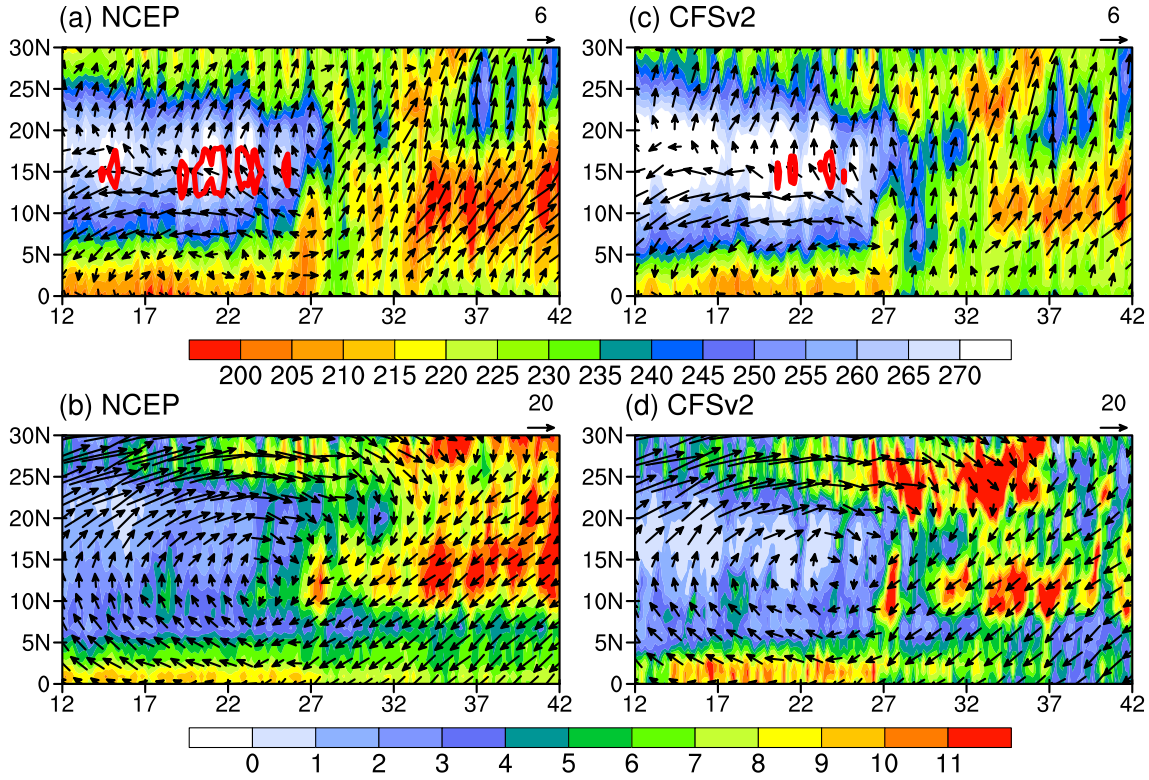

Fig. 1. Time-latitude cross-sections of daily values of (a, c) OLR (shaded) and 850-hPa winds (vectors; m s^{-1}) and (b, d) precipitation (shaded; mm d^{-1}) and 200-hPa winds (vectors; m s^{-1}) along 110°–120°E from the 12th pentad to the 42nd pentad (*x*-axis) for the NCEP–NCAR reanalysis and the CFSv2 LD0, respectively. Red bold lines in (a) and (c) are the 5880 gpm geopotential heights.

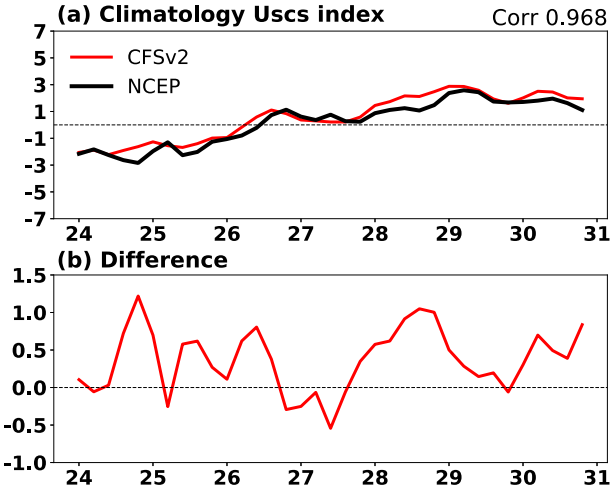

Fig. 2. (a) Temporal curves of daily SCSSM index from the 24th pentad to 30th pentad (*x*-axis) for the NCEP–NCAR observations (black solid line), its yearly mean values, and the CFSv2 LD0 projection (red solid line). (b) Difference in daily SCSSM index between the NCEP–NCAR and CFSv2 LD0 (the latter minus the former).

accompanied by the enhancement of southwesterly winds from the equatorial IO to the SCS, leading to an eastward extension of the westerlies to the SCS (Fig. 3c). The Bay of Bengal SST decreases and the SST to the east of the Philippines increases during the SCSSMO (right panels of Fig. 3), also contributing to westerlies irrupt into the SCS. Meanwhile, a strengthening and northeastward shift of the South Asian high and weakening of the westerly jet are observed during the SCSSMO (Fig. 3f). As a result, convection and heavy rainfall occur over the southern SCS (Figs. 3b and 3f). After the SCSSMO, southwesterly winds dominate over the SCS, accompanied by convection and rainfall expanding northward to South China (Figs. 3c and 3g). This onset process is consistent with previous studies (Lau and Yang, 1997; Ding and Sun, 2001; Ding and Chan, 2005; Li et al., 2020).

The time-latitude cross-section of the climatological SCSSMO process along 110°–120°E in the CFSv2 LD0 is presented in Figs. 1c–d. At LD0, the model generally reproduces the evolution of atmospheric circulation, including the reversal of 850-hPa winds from easterlies to westerlies over the latitudinal bands of SCS around the 27th pentad, and the weakening of 200-hPa westerly winds from the 12th pentad to the 32nd pentad to the north of 20°N. Enhancement of precipitation and convection over the SCS during the SCSSMO is also captured well by the model. On the other hand, the CFSv2 overestimates the rainfall (convection) to the north of 20°N after the SCSSMO and underestimates the rainfall (convection) over the SCS after the 32nd pentad (Fig. 1), which may be associated with the biases of low-level southwesterly wind forecasts (Zhao and Yang, 2014). Overall, the model generally captures the major features associated with the SCSSMO process, particularly for the climatological onset time around the 27th pentad. The accurate prediction of the SCSSMO date by the CFSv2 LD0 can be also verified in Fig. 2a, where the red solid line denotes the climatological daily SCSSM index for the CFSv2 LD0. The sub-seasonal variation of the SCSSM index in LD0 is generally similar to that in the observations (Fig. 2a). The observed index value changes from negative to positive around the 27th pentad and this is successfully captured by the model. However, the daily SCSSM index in LD0 is overestimated compared to that in observation except around the onset pentad (Fig. 2b).

The sub-seasonal evolutions of convection, precipitation, atmospheric circulation, and SST around the SCSSMO are displayed in Fig. 4. The model captures the major features of SCSSMO evolution, namely the retreat of the WNPSH, the development of southwesterly monsoon flow, and the increase in the east-west SST gradient from the 25th pentad to the 29th pentad (Figs. 3 and 4). Furthermore, the northward shift of the rain belt arc mimics that in observations (Figs. 3d and 4d). However, weaker-than-observed convection appears from the IO to the Maritime Continent during the 25th–29th pentads (Figs. 4b–c), accompanied by less-than-observed rainfall over the equatorial IO from the 25th pentad to the 29th pentad (Figs. 4e, f, g), as well as the rainfall over the SCS at the 29th pentad. Besides, the model realistically reproduces the upper-level circulation and the SST patterns (Figs. 3 and 4). However, the WNPSH in the CFSv2 is weaker than that in observation, consistent with the result of Jiang et al. (2013).

4. Prediction of the climatological SCSSMO at different time leads

Figure 5 presents the climatological pentad-mean SCSSM index from the 24th to 30th pentads for observation and the CFSv2 predictions of different leads of time. The evolution of the SCSSM index is generally captured by the model at all lead times, but the date of SCSSMO is accurately predicted only within one pentad lead. When lead time is longer than that, the predicted onset date is 1–2 pentads earlier than the observed. A noteworthy overestimation of the SCSSM index before the 27th pentad can be found when lead time is longer than one pentad, which contributes to the earlier SCSSMO in the model. Besides, the predicted SCSSM index increases (decreases) before (after) the 27th pentad as lead time increases, resulting in a less conspicuous SCSSMO compared to that observed (Fig. 5). Specifically, the predicted earlier-than-observed SCSSMO after 1-pentad lead can be primarily attributed to the underestimation of easterlies (or westerly bias) over the SCS before the SCSSMO, while the weaker-than-observed SCSSMO stems from the underestimations of easterlies and westerlies at the pre-SCSSMO after 1-pentad lead and at the post-SCSSMO after 31-day lead, respectively (Fig. 5).

We further analyze the skill of the NCEP CFSv2 in predicting the atmospheric and oceanic processes at the pre-SCSSMO and the post-SCSSMO. Figure 6 presents the

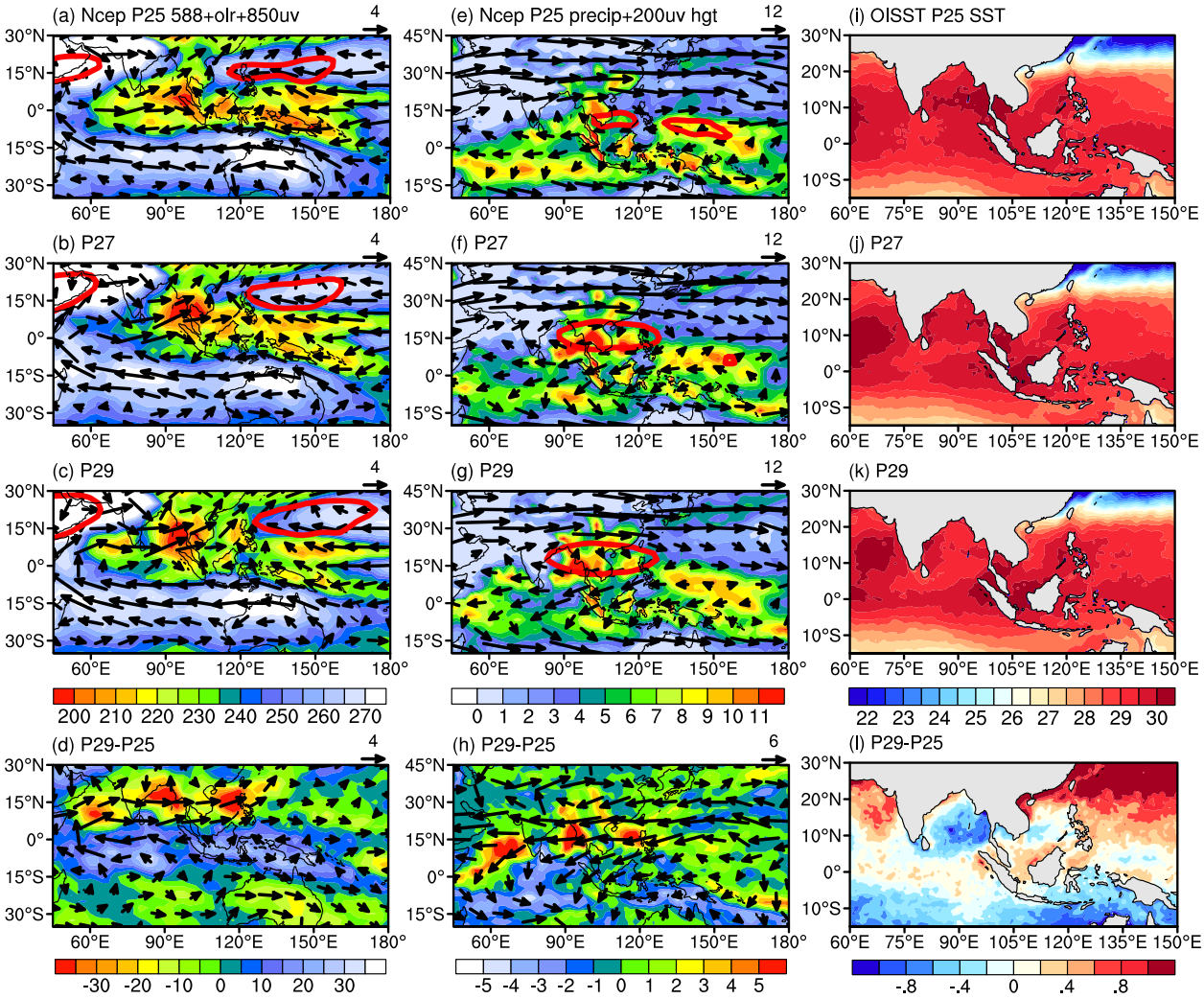

Fig. 3. NCEP–NCAR 850-hPa winds (vectors; m s^{-1}) and OLR (shaded) in (a) the 25th pentad, (b) the 27th pentad, (c) the 29th pentad and (d) differences between the 29th pentad and the 25th pentad. (e)–(h) and (i)–(l) as in (a)–(d), but for 200-hPa winds and precipitation, and SST, respectively. Red bold lines in (a)–(c) and (e)–(g) are the 5880 and 12 488 gpm geopotential heights, respectively.

differences in SST and 850-hPa winds at the 24th pentad and the 29th pentad between the CFSv2 predictions and observations in different leads. At the pre-SCSSMO, there is negligible bias (less than 0.2°C) between the observed and predicted SSTs within 1-pentad lead (Figs. 6a–b). The predicted large-scale atmospheric circulation is generally consistent with that observed. However, when the lead time is longer than 6 days, notable warm biases appear in the equatorial western Pacific (Figs. 6c–e), accompanied by enhanced rainfall (Figs. 3e and 4e). As a result, there is a cyclonic circulation bias over the WNP, which can be regarded as a Rossby wave response to latent heating (Matsuno, 1966; Gill, 1980; Hu et al., 2020a). This cyclonic circulation bias demonstrates that the model predicts a weaker-than-observed WNPSH, favoring an earlier eastward retreat of the WNPSH and weaker low-level easterlies over the SCS in the CFSv2, both of which contribute to an earlier and less forceful SCSSMO at longer leads. After the SCSSMO, warm biases in the equatorial western Pacific and the SCS accumulate rapidly before LD26, accompanied by a cyclonic circulation bias over the WNP, leading to an overestimation of westerlies over the SCS (right panels in Fig. 6). When lead time is longer than 31 days, large warm biases appear in the eastern IO. Consequently, warm biases over the eastern IO-SCS, together with cold biases over the WNP, induce easterly biases over the SCS in longer leads. These easterly biases signify weaker-than-observed westerlies at the post-SCSSMO, further contributing to the underestimation of the SCSSMO.

Figure 7 presents 500-hPa geopotential height averaged over the WNP (125°–180°E, 15°–20°N) in the 25th (black), 27th (red) and 29th (blue) pentads from observation and the CFSv2 LD0–LD40. The WNPSH strengthens east of the Philippines from the 25th pentad to the 29th pentad, consistent with the eastward shift of the WNPSH during the SCSSMO. This feature is well captured by the model in all leads. However, the WNPSH in the CFSv2 is weaker than observed during the SCSSMO. The predicted WNPSH rapidly weakens

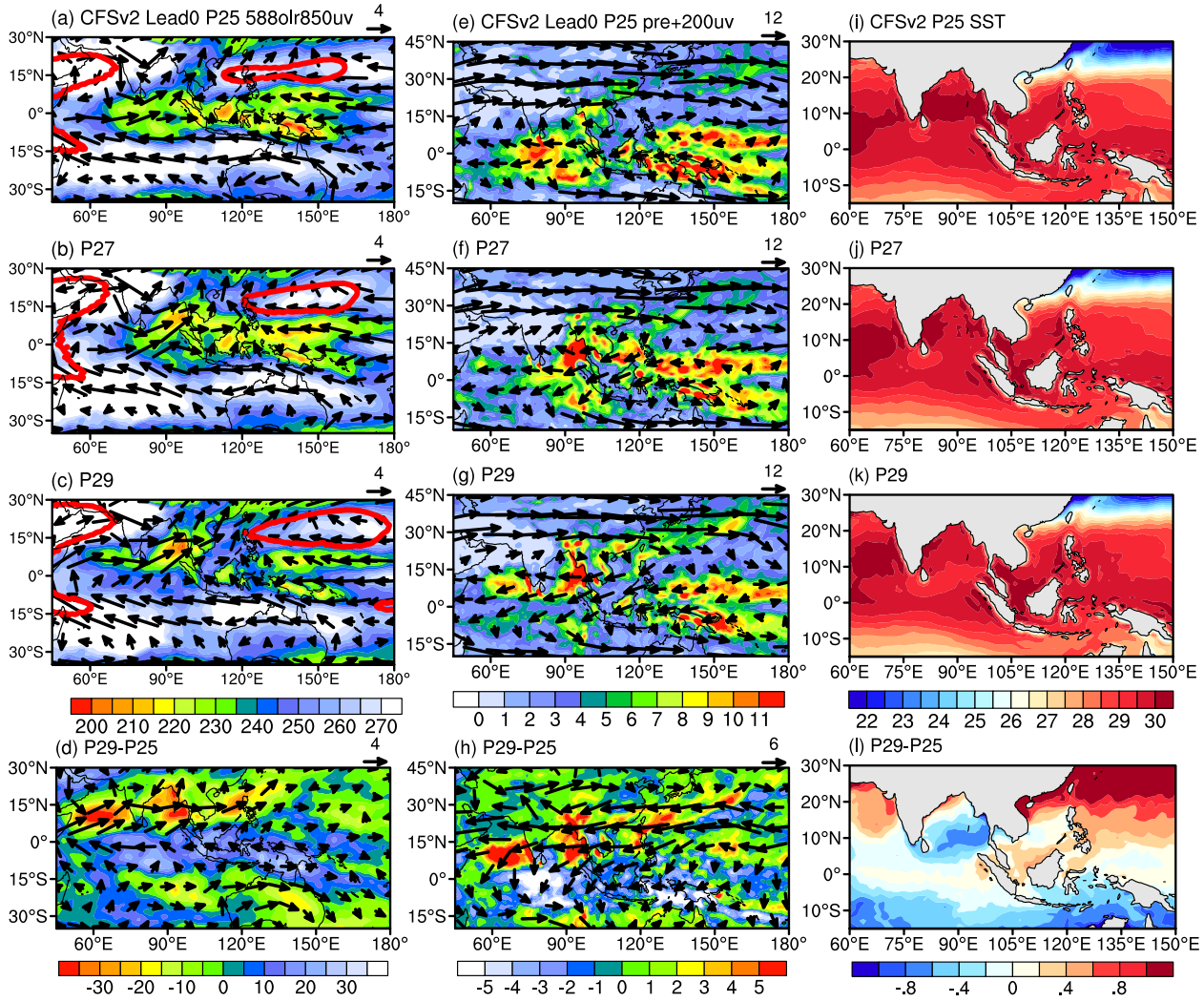

Fig. 4. As in Fig. 3, but for the CFSv2 LD0. Red bold lines in (a)–(c) are the 5872 gpm geopotential heights, respectively.

as lead time increases, consistent with the quickly enhanced cyclonic bias over the WNP (Figs. 6b–e and Fig. 7).

5. Sub-seasonal prediction of the SCSSMO cases in the NCEP CFSv2

Figure 8 displays the SCSSMO dates in the CFSv2 hindcast and the reanalysis, identified by the method proposed by Wang et al. (2004). In observations, the date of SCSSMO varies greatly from year to year, with the earliest (latest) onset occurring in the 24th (33rd) pentad. During the 16 years analyzed, the model successfully predicts the onset date in 10 years at LD0 (Fig. 8a). The CFSv2 slightly overestimates the SCSSM index at LD0 (Fig. 2); however, in four years the onset date in the model is later than the observed (Fig. 8). The number of advanced onset dates increases from LD1 to LD21 and decreases after LD26, consistent with the climatological SCSSM index biases. On the other hand, the predicted onset pentad varies in different lead days, with the largest discrepancy of predicted onset pentad in 2006 (Fig. 8). The prediction skills differ greatly year by year, which is possibly linked to the intensity of the SCSSMO.

To investigate the predictability of the SCSSMO, we analyze the temporal evolution of the pentad SCSSM index from the 20th to 39th pentads in different years. The CFSv2 generally captures the evolutionary features of the SCSSM index in LD0 and shows better performance in simulating the SCSSM index evolutionary process than predicting the SCSSMO date, according to the criterion of Wang et al. (2004) (figures not shown). In addition, it is found that the model can accurately predict the evolution of the index as well as the SCSSMO date more than two weeks in advance in some years, while the performance is poor in other years. As an example, Fig. 9 presents the temporal curves of the pentad SCSSM index in 2003 and 2012. The index is increasingly overestimated before the SCSSMO as lead time increases (Figs. 9a–f) and underestimated after the SCSSMO from LD21 to LD41 (figures not shown) in the CFSv2. Before LD21, the model can accurately predict the SCSSMO process (Figs. 9a–d) and capture the onset time (Figs. 8a–d). However, for 2012, the model can only well reproduce the evolu-

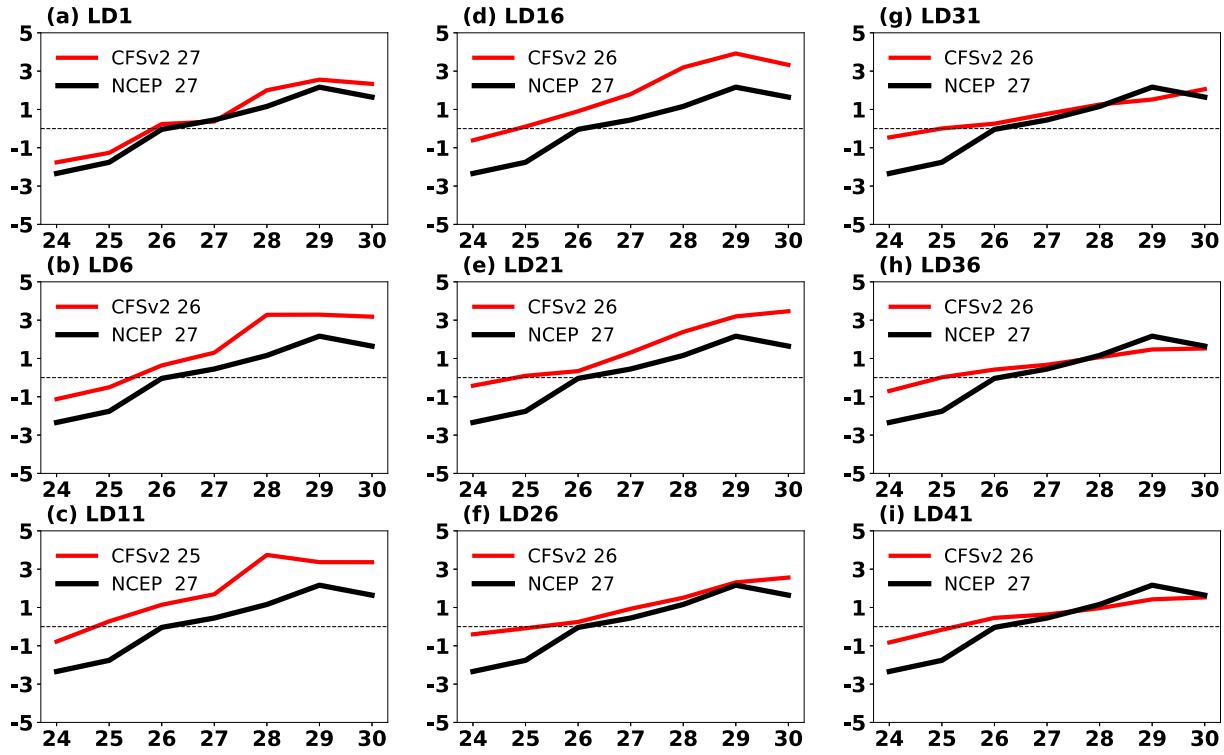

Fig. 5. Temporal curves of pentad mean SCSSM index from the 24th pentad to the 30th pentad (*x*-axis) for the NCEP–NCAR observational analysis (black solid lines) and the CFSv2 projection (red solid lines) in (a) LD1, (b) LD6, (c) LD11, (d) LD16, (e) LD21, (f) LD26, (g) LD31, (h) LD36 and (i) LD41.

tion of the index within a period of just five lead days (Fig. 9g). Obviously, there is a distinct feature of the SCSSMO between 2003 and 2012, namely the intensity of the SCSSMO, which is defined as the post-onset second pentad SCSSM index minus the pre-onset second pentad SCSSM index. A larger (smaller) value of the intensity of the SCSSMO is referred to as a more (less) vigorous or forceful monsoon onset process. The above-described relationship between the SCSSMO prediction skill and the SCSSMO intensity is also found in other years (figures not shown).

The prediction skill of SCSSMO as a function of the SCSSMO intensity is presented in Fig. 10. The prediction skill represents the maximum lead days that the CFSv2 can capture the SCSSMO process (defined as the temporal correlation coefficient of the index exceeding 0.8 and root-mean-square error being below 3.3 between observations and prediction from the 24th pentad to the 34th pentad) in each year. The results are not sensitive to the thresholds of correlation coefficient and root-mean-square error. The prediction skill of the NCEP CFSv2 exceeds 20 days for the largest intensity of SCSSMO. The CFSv2 can predict SCSSMO date around two weeks in advance when the SCSSM onset intensity is greater than 11 m s^{-1}. The prediction skill decays rapidly afterward. The onset date can only be accurately predicted by the model within one week when the onset intensity is smaller than 6 m s^{-1}. In general, a vigorous SCSSMO process shows higher predictability, and vice versa. Among the four years that the CFSv2 predicted the SCSSMO date two weeks in advance, there is one El Niño year (2003), one La Niña year (2008), and two normal years (2002 and 2004). In addition, low skills are observed to follow normal winters and strong ENSO events. There is no apparent relationship between the predictability of the SCSSMO and ENSO.

6. Summary and discussion

The SCSSMO and its associated atmospheric and oceanic processes are important indicators for the seasonal transition of East Asia climate. The NCEP CFSv2 provides important information for the sub-seasonal prediction of the SCSSMO. In this study, we have provided a comprehensive assessment of the sub-seasonal prediction and predictability of the SCSSMO, focusing on their climatic characteristics and unique features of different cases.

Regarding the climatological means (1999–2014), the SCSSMO occurs around the 27th pentad. The SCSSMO is accompanied by an eastward retreat of the WNPSH, weakening of the westerly jet stream, and intensified South Asian High. Besides, SST decreases in the Bay of Bengal and increases to the east of the Philippines during the SCSSMO, leading to an increase in the east-west SST gradient. These changes in atmospheric circulation and SST favor the onset of westerlies and strengthen convection and precipitation over the SCS.

The NCEP CFSv2 LD0 accurately captures the SCSSMO date and the major features associated with SCSSMO evolution. The transition of atmospheric circulation and the enhancement of rainfall and convection in the

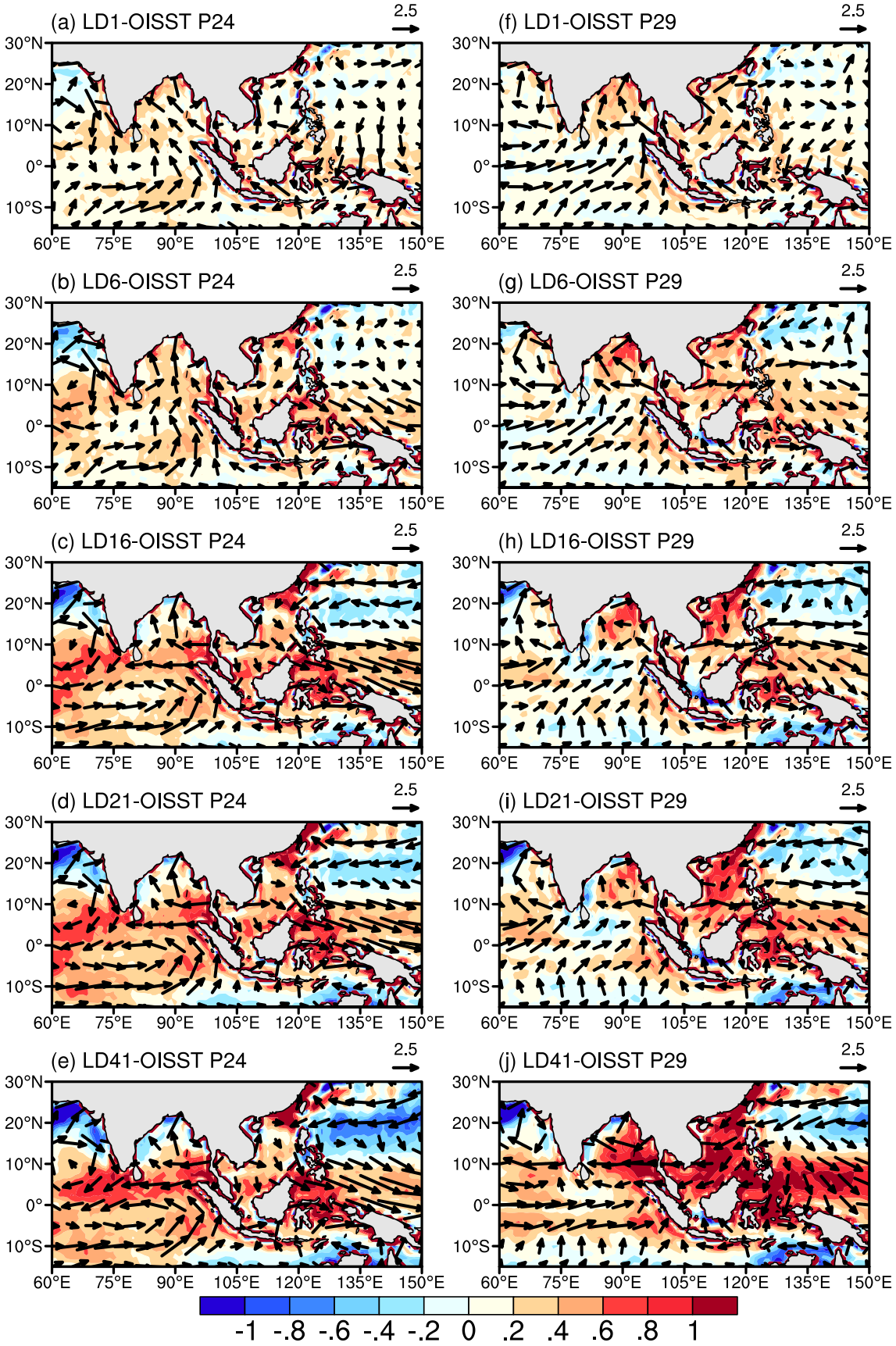

Fig. 6. Differences in SST (shaded; °C) and 850-hPa winds (vectors; m s^{-1}) between observations and the CFSv2 predictions in (a) and (f) LD1, (b) and (g) LD6, (c) and (h) LD16, (d) and (i) LD21, and (e) and (j) LD41 (the CFSv2 minus observations) at the 24th pentad (left) and the 29th pentad (right).

model simulations are similar to those in observations. However, the daily SCSSM index in LD0 is overestimated compared to the observed except around the onset pentad. This may be attributed to an underestimation of the WNPSH intensity, which can modulate the westerlies over the SCS and lead to overestimated SCSSM indexes.

Climatologically, the NCEP CFSv2 can capture the general evolution features of the SCSSMO at all lead times, but it can only accurately predict the SCSSMO date one pentad in advance. When lead time is longer than one pentad, the predicted onset date would be 1–2 pentads earlier compared to observation, which can be attributed to an underestimation of easterlies (or westerly bias) over the SCS before the SCSSMO. Besides, the predicted SCSSM index unrealistically increases (decreases) before (after) the 27th pentad as lead time increases, resulting in a less conspicuous SCSSMO compared to that observed. Several causes can be possibly responsible for the growth of those biases. On the one hand, before the SCSSMO, warmer-than-observed SST with positive rainfall bias appears over the equatorial western Pacific when lead time is longer that one pentad, producing a Rossby wave response to the latent heating. Thus, a cyclonic circulation bias is observed over the WNP, signifying a weaker-than-observed WNPSH. This weaker WNPSH leads to a weakening of the low-level easterlies over the SCS and favors an earlier eastward retreat of the WNPSH in the CFSv2, both of which contribute to an earlier and less forceful SCSSMO. On the other hand, after the SCSSMO, pronounced warm biases appear over the eastern IO-SCS, together with cold biases over the WNP, inducing easterly biases over the SCS. These easterly biases signify weaker-than-observed westerlies during the SCSSMO, further contributing to the underestimation of the SCSSMO. Apparently, the SST biases over the IO and the western Pacific jointly regulate the atmospheric circulation, through the air-sea interaction, and hence the SCSSMO in the NCEP CFSv2.

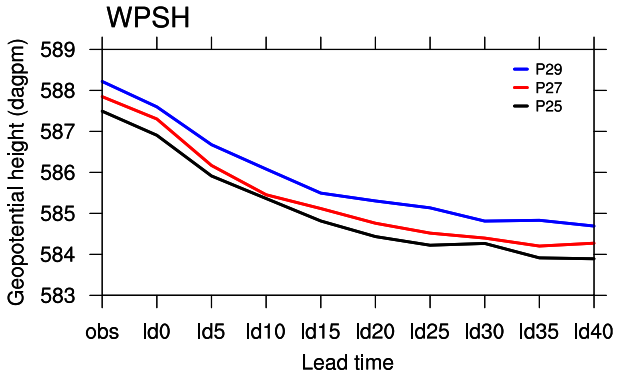

Fig. 7. Area-averaged 500-hPa geopotential height over the WNP (125°–180°E, 15°–20°N, solid line) at the 25th (black), the 27th (red) and the 29th (blue) pentads in the observations and the CFSv2 predictions from LD0 to LD40.

The skill of the NCEP CFSv2 in predicting the SCSSMO differs greatly year by year, related to the predictability of the SCSSMO in individual years. The CFSv2 shows a better performance in predicting the SCSSM index evolution than the SCSSMO date, with an increase in lead time. It can predict both the evolution of the index and the SCSSMO date more than two weeks in advance in some years, while the performance is poor in other years. The model can successfully predict the SCSSMO up to 18 days in advance for the most vigorous SCSSMO, while it can only reproduce the SCSSMO within one pentad for the least powerful SCSSMO. The prediction skill decays as the

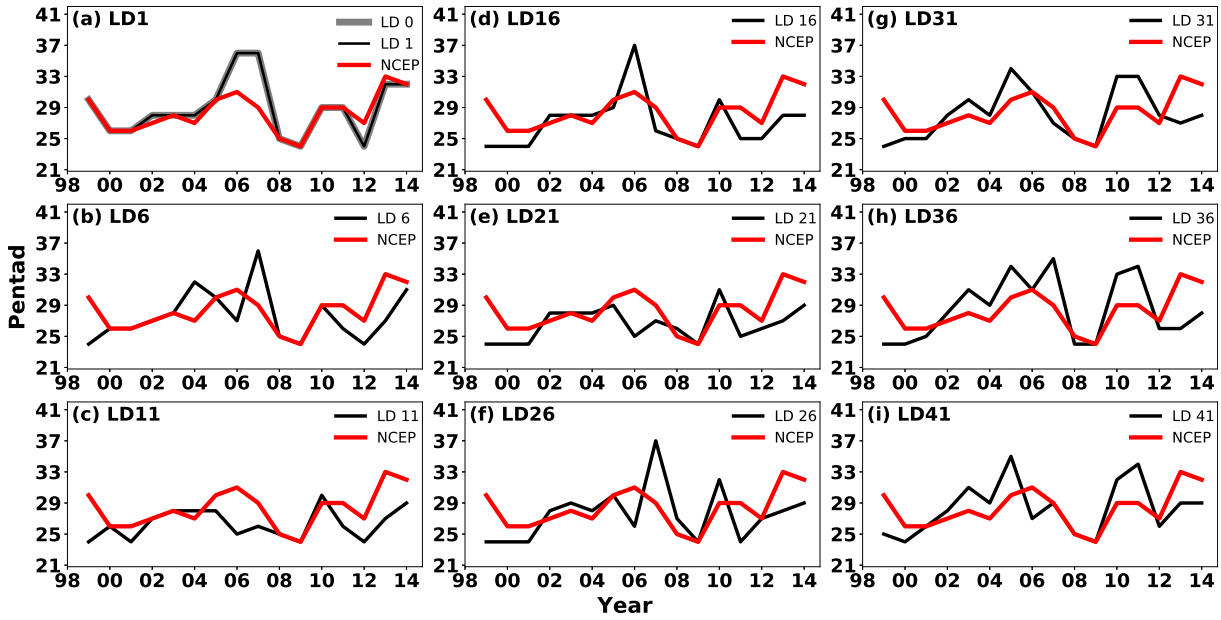

Fig. 8. Onset pentads derived using the method proposed by Wang et al. (2004) from 1999–2014 in the NCEP–NCAR observational analysis (red solid line), superimposed with the CFSv2 projection for (a) LD0 (grey solid lines), and the (a–i) LD1, LD6, …, and LD41 (black solid lines).

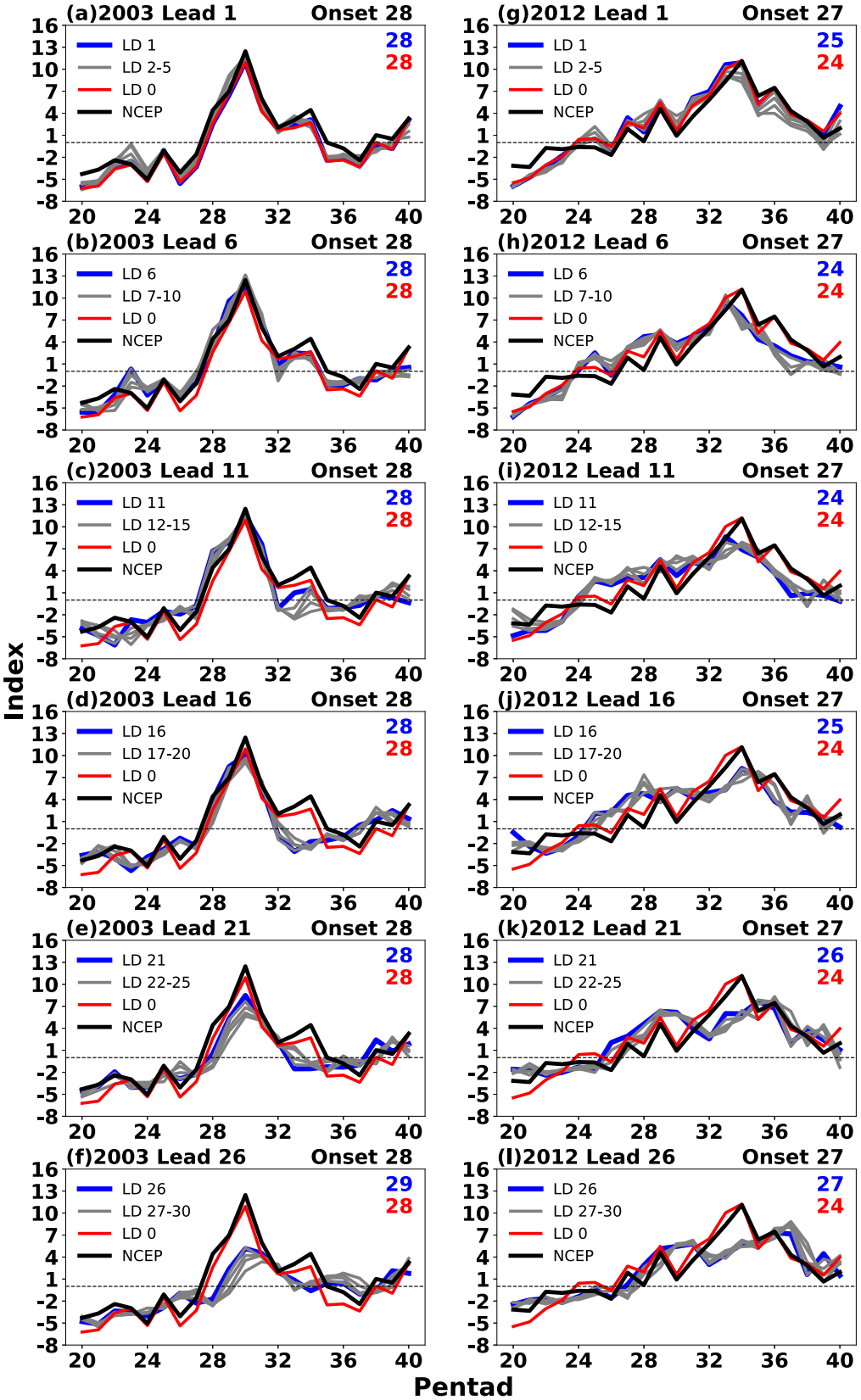

Fig. 9. Temporal curves of the pentad mean SCSSM index from the 20th pentad to the 39th pentad (*x* axis) in 2003 (left) and 2012 (right) for the NCEP–NCAR observational analysis (black), the CFSv2 LD0 projection (red) and the CFSv2 projections in (a, g) LD1, (b, h) LD6, (c, i) LD11, (d, j) LD16, (e, k) LD21 and (f, l) LD26 (blue). Onset pentads for the NCEP–NCAR are in black, the CFSv2 LD0 is shown in red and the CFSv2 predictions in the different lead times are displayed in blue.

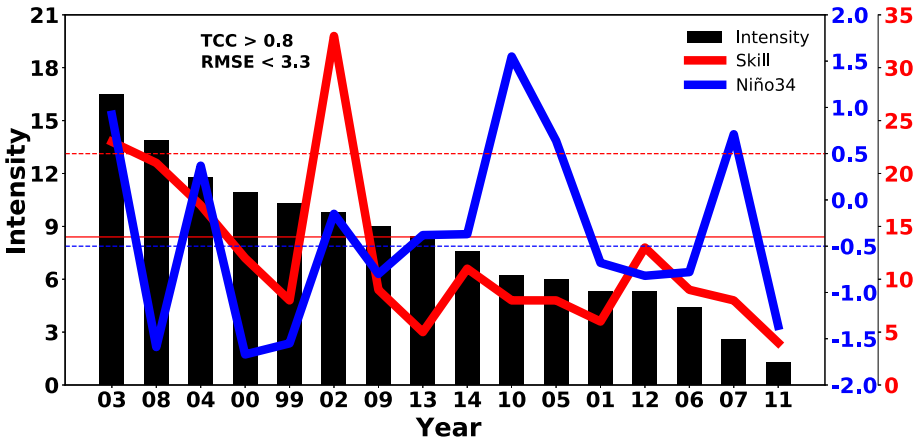

Fig. 10. Prediction skill (thick red line; day) of the SCSSMO as a function of the SCSSMO intensity (defined as the post-onset second pentad SCSSM index minus the pre-onset second pentad SCSSM index; black bars; m s^{-1}). The solid horizontal line represents a two-week prediction skill. The thick blue line represents the Niño-3.4 index in the previous winter and the dashed horizontal line isolates the index (El Niño > 0.5 and La Niña <−0.5).

SCSSMO intensity decreases. In other words, a vigorous SCSSMO process exhibits a higher predictability, and vice versa. This may provide a useful indicator for the real-time monitoring and prediction of the SCSSMO, although the assessment methods in this study may lead to an overestimation of the model prediction skill compared to real-time forecasts. It is possible to obtain higher forecasting skills for the SCSSMO, in vigorous monsoon onset years, and by improving the model's performance in prediction of the WNPSH and the IO and western Pacific SSTs.

It should be realized that the onset and evolution of the SCSSM are complex processes. The ability of model simulations shows the mean state dependence, and the associated anomalous SST patterns. The NCEP CFSv2 performs differently in predicting the eastern and central Pacific ENSO events and their climate effects (Yang and Jiang, 2014). Thus, the sub-seasonal prediction of the SCSSMO depends on the simulations of background atmospheric circulations and SST patterns on sub-seasonal time scales. To understand how the mean state affects the predictability of the SCSSMO in the CFSv2 requires further investigation. In addition, previous studies have revealed that the SCSSMO is relevant to the intraseasonal oscillation such as the Madden–Julian Oscillation (MJO) and the quasi-biweekly oscillation (Jia et al., 2013; Li et al., 2020). The CFSv2 shows relatively lower skills in predicting the enhanced convection over the Maritime Continent and the MJO, primarily contributing to its poor skill over the IO on sub-seasonal time scales (Wang et al., 2014; Dong et al., 2020; Schreck et al., 2020). The performance of the CFSv2 in predicting the MJO may affect the predictability of the SCSSMO, which warrants further investigations.

Acknowledgements. The authors thank the two anonymous reviewers and the associate editors-in-chief for the constructive comments on the earlier version of the manuscript. This research was jointly supported by the Guangdong Major Project of Basic and Applied Basic Research (Grant No. 2020B0301030004), the National Natural Science Foundation of China (Grant Nos. 42088101, 41975074 and 42175023), the Strategic Priority Research Program of the Chinese Academy of Sciences (XDA20100304), the Second Comprehensive Scientific Investigation on the Tibetan Plateau of China (2019QZKK0208), and the Guangdong Province Key Laboratory for Climate Change and Natural Disaster Studies (Grant No. 2020B1212060025).

REFERENCES

Chen, L. X., and Y. H. Wang, 1998: Numerical experiment of impact of sea surface temperature in South China Sea and warm pool/west Pacific on East Asian summer monsoon. *Journal of Meteorological Research*, **12**, 162–176.

Chen, Y. L., and D. X. Hu, 2003: The relation between the South China Sea summer monsoon onset and the heat content variations in the tropical western Pacific warm pool region. *Acta Oceanologica Sinica*, **25**, 20–31. (in Chinese with English abstract)

Ding, Y. H., and Y. Sun, 2001: A study on anomalous activities of East Asian summer monsoon during 1999. *J. Meteor. Soc. Japan*, **79**, 1119–1137, https://doi.org/10.2151/jmsj.79.1119.

Ding, Y. H., and J. C. L. Chan, 2005: The East Asian summer monsoon: An overview. *Meteorol. Atmos. Phys.*, **89**, 117–142, https://doi.org/10.1007/s00703-005-0125-z.

Ding, Y. H., C. Y. Li, and Y. J. Liu, 2004: Overview of the South China Sea monsoon experiment. *Adv. Atmos. Sci.*, **21**, 343–360, https://doi.org/10.1007/BF02915563.

Dong, S. R., S. Yang, X. Yan, T. T. Zhang, Y. R. Feng, and P. Hu, 2020: The most predictable patterns and prediction skills of subseasonal prediction of rainfall over the Indo-Pacific regions by the NCEP climate forecast system. *Climate Dyn.*, **54**, 2759–2775, https://doi.org/10.1007/s00382-020-05141-5.

Ek, M. B., K. E. Mitchell, Y. Lin, E. Rogers, P. Grunmann, V. Koren, G. Gayno, and J. D. Tarpley, 2003: Implementation of Noah land surface model advances in the National Centers

for Environmental Prediction operational mesoscale Eta model. *J. Geophys. Res.*, **108**, 8851, https://doi.org/10.1029/2002JD003296.

Gao, H., S. Yang, A. Kumar, Z.-Z. Hu, B. H. Huang, Y. Q. Li, and B. Jha, 2011: Variations of the East Asian mei-yu and simulation and prediction by the NCEP Climate Forecast System. *J. Climate*, **24**, 94–108, https://doi.org/10.1175/2010JCLI3540.1.

Geen, R., 2021: Forecasting South China Sea monsoon onset using insight from theory. *Geophys. Res. Lett.*, **48**, e2020GL091444, https://doi.org/10.1029/2020GL091444.

Gill, A. E., 1980: Some simple solutions for heat-induced tropical circulation. *Quart. J. Roy. Meteor. Soc.*, **106**, 447–462, https://doi.org/10.1002/QJ.49710644905.

Griffies, S. M., M. J. Harrison, R. C. Pacanowski, and A. Rosati, 2003. A technical guide to MOM4. GFDL Ocean group technical report No. 5. NOAA/GFDL, Princeton, 337 pp.

He, Z. Q., and R. G. Wu, 2013: Seasonality of interannual atmosphere–ocean interaction in the South China Sea. *Journal of Oceanography*, **69**, 699–712, https://doi.org/10.1007/S10872-013-0201-9.

Hu, P., W. Chen, S. F. Chen, and R. P. Huang, 2020a: Statistical analysis of the impacts of intra-seasonal oscillations on the South China Sea summer monsoon withdrawal. *International Journal of Climatology*, **40**, 1919–1927, https://doi.org/10.1002/joc.6284.

Hu, P., W. Chen, S. F. Chen, Y. Y. Liu, and R. P. Huang, 2020b: Extremely early summer monsoon onset in the South China Sea in 2019 following an El Niño event. *Mon. Wea. Rev.*, **148**, 1877–1890, https://doi.org/10.1175/MWR-D-19-0317.1.

Jia, X. J., C. Zhang, R. G. Wu, and Q. F. Qian, 2021: Changes in the relationship between spring precipitation in southern China and Tropical Pacific-South Indian Ocean SST. *J. Climate*, **34**, 6267–6279, https://doi.org/10.1175/JCLI-D-20-0817.1.

Jia, X. L., S. Yang, X. Li, Y. Y. Liu, H. Wang, X. W. Liu, and S. Weaver, 2013: Prediction of global patterns of dominant quasi-biweekly oscillation by the NCEP Climate Forecast System version 2. *Climate Dyn.*, **41**, 1635–1650, https://doi.org/10.1007/s00382-013-1877-7.

Jiang, X. W., S. Yang, Y. Q. Li, A. Kumar, W. Q. Wang, and Z. T. Gao, 2013: Dynamical prediction of the East Asian winter monsoon by the NCEP climate forecast system. *J. Geophys. Res.*, **118**, 1312–1328, https://doi.org/10.1002/jgrd.50193.

Kajikawa, Y., and B. Wang, 2012: Interdecadal change of the South China Sea summer monsoon onset. *J. Climate*, **25**, 3207–3218, https://doi.org/10.1175/jcli-d-11-00207.1.

Kalnay, E., and Coauthors, 1996: The NCEP/NCAR 40-year reanalysis project. *Bull. Amer. Meteor. Soc.*, **77**, 437–472, https://doi.org/10.1175/1520-0477(1996)077<0437:TNYRP>2.0.CO;2.

Lau, K. M., and S. Yang, 1997: Climatology and interannual variability of the Southeast Asian summer monsoon. *Adv. Atmos. Sci.*, **14**, 141–162, https://doi.org/10.1007/s00376-997-0016-y.

Lau, K.-M., H.-T. Wu, and S. Yang, 1998: Hydrologic processes associated with the first transition of the Asian summer monsoon: A pilot satellite study. *Bull. Amer. Meteor. Soc.*, **79**, 1871–1882, https://doi.org/10.1175/1520-0477(1998)079<1871:HPAWTF>2.0.CO;2.

Li, C., S. Yang, W. Mo, and J. Zhang, 2022: Seasonal prediction for May rainfall over southern China based on the NCEP CFSv2. *Journal of Tropical Meteorology*, **28**, 29–44, https://doi.org/10.46267/j.1006-8775.2022.003.

Li, Y., S. Yang, Y. Deng, and B. Zheng, 2020: Signals of spring thermal contrast related to the interannual variations in the onset of the South China Sea summer monsoon. *J. Climate*, **33**, 27–38, https://doi.org/10.1175/JCLI-D-19-0174.1.

Liang, J. Y., S. Yang, Z. Z. Hu, B. H. Huang, A. Kumar, and Z. Q. Zhang, 2009: Predictable patterns of the Asian and Indo-Pacific summer precipitation in the NCEP CFS. *Climate Dyn.*, **32**, 989–1001, https://doi.org/10.1007/s00382-008-0420-8.

Lin, A. L., and R. H. Zhang, 2020: Climate shift of the South China Sea summer monsoon onset in 1993/1994 and its physical causes. *Climate Dyn.*, **54**, 1819–1827, https://doi.org/10.1007/s00382-019-05086-4.

Liu, B. Q., and C. W. Zhu, 2019: Extremely late onset of the 2018 South China Sea summer monsoon following a La Niña event: Effects of triple SST anomaly mode in the North Atlantic and a weaker mongolian cyclone. *Geophys. Res. Lett.*, **46**, 2956–2963, https://doi.org/10.1029/2018gl081718.

Liu, B. Q., and C. W. Zhu, 2020: Boosting effect of tropical cyclone "Fani" on the onset of the South China Sea summer monsoon in 2019. *J. Geophys. Res.*, **125**, e2019JD031891, https://doi.org/10.1029/2019JD031891.

Liu, B. Q., and C. W. Zhu, 2021: Subseasonal-to-seasonal predictability of onset dates of South China Sea summer monsoon: A perspective of meridional temperature gradient. *J. Climate*, **34**, 5601–5616, https://doi.org/10.1175/JCLI-D-20-0696.1.

Liu, X. W., S. Yang, A. Kumar, S. Weaver, and X. W. Jiang, 2013: Diagnostics of subseasonal prediction biases of the Asian summer monsoon by the NCEP climate forecast system. *Climate Dyn.*, **41**, 1453–1474, https://doi.org/10.1007/s00382-012-1553-3.

Martin, G. M., A. Chevuturi, R. E. Comer, N. J. Dunstone, A. A. Scaife, and D. Q. Zhang, 2019: Predictability of South China Sea summer monsoon onset. *Adv. Atmos. Sci.*, **36**, 253–260, https://doi.org/10.1007/s00376-018-8100-z.

Matsuno, T., 1966: Quasi-geostrophic motions in the equatorial area. *J. Meteor. Soc. Japan*, **44**, 25–43, https://doi.org/10.2151/jmsj1965.44.1_25.

Moorthi, S., H.-L. Pan, and P. Caplan, 2001: Changes to the 2001 NCEP operational MRF/AVN global analysis/forecast system. NWS Technical Procedures Bulletin 484, 1–14.

Reynolds, R. W., T. M. Smith, C. Y. Liu, D. B. Chelton, K. S. Casey, and M. G. Schlax, 2007: Daily high-resolution-blended analyses for sea surface temperature. *J. Climate*, **20**, 5473–5496, https://doi.org/10.1175/2007JCLI1824.1.

Saha, S., and Coauthors, 2014: The NCEP climate forecast system version 2. *J. Climate*, **27**, 2185–2208, https://doi.org/10.1175/JCLI-D-12-00823.1.

Schreck, C. J., M. A. Janiga, and S. Baxter, 2020: Sources of tropical subseasonal skill in the CFSV2. *Mon. Wea. Rev.*, **148**, 1553–1565, https://doi.org/10.1175/MWR-D-19-0289.1.

Tao, S. Y., and L. X. Chen, 1987: A review of recent research on the East Asian summer monsoon in China. *Monsoon Meteorology*, C.-P. Chang and T. N. Krishnamurti, Eds., Oxford University Press, 60–92.

Wang, B., LinHo, Y. S. Zhang, and M.-M. Lu, 2004: Definition of South China Sea monsoon onset and commencement of the East Asia summer monsoon. *J. Climate*, **17**, 699–710,

https://doi.org/10.1175/2932.1.

Wang, B., J. Yang, T. J. Zhou, and B. Wang, 2008: Interdecadal changes in the major modes of Asian-Australian monsoon variability: Strengthening relationship with ENSO since the late 1970s. *J. Climate*, **21**, 1771–1789, https://doi.org/10.1175/2007JCLI1981.1.

Wang, B., F. Huang, Z. W. Wu, J. Yang, X. H. Fu, and K. Kikuchi, 2009: Multi-scale climate variability of the South China Sea monsoon: A review. *Dyn. Atmos. Oceans*, **47**, 15–37, https://doi.org/10.1016/j.dynatmoce.2008.09.004.

Wang, B., and Coauthors, 2021: Monsoons climate change assessment. *Bull. Amer. Meteor. Soc.*, **102**, E1–E19, https://doi.org/10.1175/BAMS-D-19-0335.1.

Wang, W. Q., M. P. Hung, S. J. Weaver, A. Kumar, and X. H. Fu, 2014: MJO prediction in the NCEP climate forecast system version 2. *Climate Dyn.*, **42**, 2509–2520, https://doi.org/10.1007/s00382-013-1806-9.

Wang, Z. Y., Y. H. Ding, M. M. Lu, B. T. Zhou, S. Yang, X. W. Jiang, and Z. J. Ke, 2017: Intraseasonal variability and predictability of the subtropical Asian summer rain band. *International Journal of Climatology*, **37**, 4119–4130, https://doi.org/10.1002/joc.5033.

Wu, C., S. Yang, A. Wang, and S. Fong, 2005: Effect of condensational heating over the Bay of Bengal on the onset of the South China Sea monsoon in 1998. *Meteorol. Atmos. Phys.*, **90**, 37–47, https://doi.org/10.1007/s00703-005-0115-1.

Wu, G. X., and Y. S. Zhang, 1998: Tibetan Plateau forcing and the timing of the monsoon onset over South Asia and the South China Sea. *Mon. Wea. Rev.*, **126**, 913–927, https://doi.org/10.1175/1520-0493(1998)126<0913:TPFATT>2.0.CO;2.

Yan, Y. H., B. Q. Liu, and C. W. Zhu, 2021: Subseasonal predictability of South China Sea summer monsoon onset with the ECMWF S2S forecasting system. *Geophys. Res. Lett.*, **48**, e2021GL095943, https://doi.org/10.1029/2021GL095943.

Yang, S., and X. W. Jiang, 2014: Prediction of eastern and central pacific ENSO events and their impacts on east asian climate by the NCEP climate forecast system. *J. Climate*, **27**, 4451–4472, https://doi.org/10.1175/JCLI-D-13-00471.1.

Yang, S., Z. Q. Zhang, V. E. Kousky, R. W. Higgins, S.-H. Yoo, J. Y. Liang, and Y. Fan, 2008: Simulations and seasonal prediction of the Asian summer monsoon in the NCEP climate forecast system. *J. Climate*, **21**, 3755–3775, https://doi.org/10.1175/2008jcli1961.1.

Zhang, T. T., S. Yang, X. W. Jiang, and S. R. Dong, 2016: Sub-seasonal prediction of the maritime continent rainfall of wet-dry transitional seasons in the NCEP climate forecast version 2. *Atmosphere*, **7**, 28, https://doi.org/10.3390/atmos7020028.

Zhao, S. Y., and S. Yang, 2014: Dynamical prediction of the early season rainfall over southern China by the NCEP Climate Forecast System. *Wea. Forecasting*, **29**, 1391–1401, https://doi.org/10.1175/WAF-D-14-00012.1.

Zhao, S. Y., S. Yang, Y. Deng, and Q. P. Li, 2015: Skills of yearly prediction of the early-season rainfall over southern China by the NCEP climate forecast system. *Theor. Appl. Climatol.*, **122**, 743–754, https://doi.org/10.1007/s00704-014-1333-6.

Zhu, Z. W., and T. Li, 2017: Empirical prediction of the onset dates of South China Sea summer monsoon. *Climate Dyn.*, **48**, 1633–1645, https://doi.org/10.1007/s00382-016-3164-x.

Zuo, Z. Y., S. Yang, Z.-Z. Hu, R. H. Zhang, W. Q. Wang, B. H. Huang, and F. Wang, 2013: Predictable patterns and predictive skills of monsoon precipitation in Northern Hemisphere summer in NCEP CFSv2 reforecasts. *Climate Dyn.*, **40**, 3071–3088, https://doi.org/10.1007/s00382-013-1772-2.